APS physics

CHORUS

This is the accepted manuscript made available via CHORUS. The article has been published as:

Kinetics of the melting front in two-dimensional plasma crystals: Complementary analysis with the particle image and particle tracking velocimetries

J. D. Williams, E. Thomas, Jr., L. Couëdel, A. V. Ivlev, S. K. Zhdanov, V. Nosenko, H. M. Thomas, and G. E. Morfill

Phys. Rev. E **86**, 046401 — Published 11 October 2012

DOI: 10.1103/PhysRevE.86.046401

Kinetics of the Melting Front in Two-Dimensional Plasma Crystals: Complementary Analysis with the Particle Image and Particle Tracking Velocimetries

J. D. Williams[1],* E. Thomas, Jr.[2], L. Couëdel[3], A. V. Ivlev[4], S. K. Zhdanov[4], V. Nosenko[4], H. M. Thomas[4], and G. E. Morfill[4]

[1] *Department of Physics, Wittenberg University, Springfield, OH 45504, USA*

[2] *Department of Physics, Auburn University, Auburn, Alabama 36849, USA*

[3] *Laboratoire PIIM, CNRS/Université d'Aix-Marseille, 13397 Marseille Cedex 20, France*

[4] *Max Planck Institute for Extraterrestrial Physics, 85741 Garching, Germany*

(Dated: August 22, 2012)

Melting of a two-dimensional plasma crystal occurring due to a mode-coupling instability is studied using particle tracking and particle image velocimetry techniques. By combining these techniques, it is possible to identify the location of a propagating melting front and find a characteristic scale length for the temperature gradient across the front. It is found that the measurements of heat transport are consistent with a simple two-dimensional model allowing us to estimate the thermal diffusivity. The measured values for the thermal diffusivity are consistent with previously measured values.

PACS numbers: 52.27.Lw, 52.27.Gr

I. INTRODUCTION

Complex plasmas are four-component plasma systems that consist of ions, electrons, neutral atoms, and charged microparticles. The charged microparticles – objects which are typically nanometer- to micrometer-sized particles that are suspended in the plasma – are an additional component of the plasma that is intimately coupled to all of the fundamental properties of the plasma. For almost three decades, these complex plasma systems have been the subject of intense study in both astrophysical [1–4] and laboratory settings [5–9]. One particular feature of complex plasmas is their ability to become self-organized into strongly coupled, two-dimensional (e.g., plasma crystals)[10, 11] or three-dimensional (e.g., Coulomb clusters) [12] structures. Here, strongly coupled refers to the fact that the Coulomb coupling parameter, Γ = electrostatic potential energy/thermal energy $\gg 1$.

Complex plasmas allow us to directly image the individual microparticles in the plasma. The large mass of the microparticles, as compared to the ions, electrons, and neutrals, means that both length and time scales of complex phenomena become stretched to hundreds of micrometers and tens of milliseconds, respectively. This allows detailed measurements to be made of complex plasma phenomena at the kinetic level using relatively straightforward diagnostic techniques, such as video imaging. When coupled with the ability to experimentally control the Coulomb coupling parameter, it is possible to study the detailed physics of transport, phase transitions, and collective behavior in plasmas. Moreover, the broad range of physical phenomena that can be explored with these systems place complex plasmas in the regime of "soft condensed matter" phenomena similar to complex fluids and granular media.

In this paper, we report on a combined analysis of two-dimensional melting in a planar plasma crystal experiment, by employing two particle tracking techniques: Particle Image Velocimetry (PIV) and Particle Tracking Velocimetry (PTV). In particular, this work focuses on the transport of heat across the temperature gradient layer that exists along a propagating melting front. The analysis presented here identifies the location of the temperature gradient region, calculates a characteristic scale length, and shows that these measurements are consistent with a generalized two-dimensional model of heat transport. In this manner, while this experiment is performed using a complex plasma, these results can be considered to be representative of a fundamental investigation of heat transport in a soft condensed matter system.

II. EXPERIMENTS AND ANALYSIS

A. Experimental setup

The experiments described in this paper were performed in a capacitively coupled radio frequency (RF) glow discharge operating at 13.56 MHz using argon gas at neutral gas pressures of $p = 0.4$ and 0.9 Pa. The RF peak-to-peak voltage V_{pp} was between 175 V and 310 V (which corresponds to a forward RF power, P, between

*Electronic address: jwilliams@wittenberg.edu

5 W and 20 W). The self-bias voltage V_{dc} v
-60 V and -130 V. The nominal plasma pa
the bulk discharge were obtained from Lang
measurements. Typical parameters for these
were an electron temperature $T_e = 2.5$ eV and
density $n_e = 2 \cdot 10^9 \mathrm{cm}^{-3}$ at $p = 0.66$ Pa and
Under these experimental conditions, a 2D
pension was formed by levitating melamine fo
(mass density, $\rho = 1510$ kg/m^3) microspher
diameter of either 8.77 μm or 9.19 μm, which
to masses of $m = 5.3 \cdot 10^{-13}$ kg or $6.1 \cdot 1$
spectively, in the sheath above the RF elec
diameter of the obtained crystalline structu
proximately 50 to 60 mm, depending upon
of injected particles ($\simeq$11000 in Exp. 1 an
Exp. 2, each with an interparticle spacing c
were in the field of view of the camera).

The microparticles were illuminated by a
laser sheet having a Gaussian profile in the
rection with a standard deviation of 75 μm (
ing to a full width at half maximum of 17
sheet thickness was approximately constant
entire plasma crystal. The particles were i
42.6 mm $\times$ 42.6 mm region with a spatial r
41.7 μm/pixels through a window at the top
ber using a Photron FASTCAM 1024 PCI c
ating at either 250 or 500 frames per second.
camera was used to monitor the quality of th
crystal. A sketch of the experimental setup
Fig. 1.

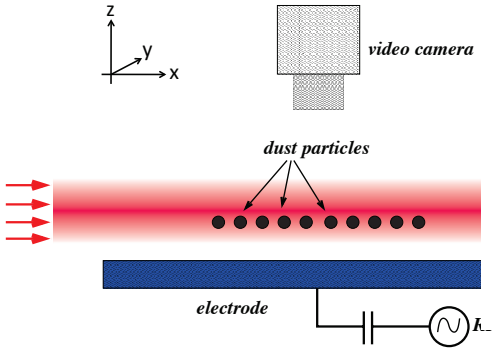

FIG. 1: (color online): Sketch of the experimental setup. Microparticles are confined above the RF electrode and illuminated with a horizontal laser sheet having a Gaussian profile in the vertical direction.

The melting of the two-dimensional plasma crystal was triggered by the mode-coupling instability [13–16, 22, 23]. This instability is driven by the coupling between two branches of the dust-lattice waves, as was predicted theoretically by Ivlev and Morfill [13] and discovered experimentally by Couëdel et al. [15]. The instability is typically induced by decreasing the neutral pressure of a gas – provided a rf discharge power is sufficiently low [16]: The reduced pressure ensures low neutral gas friction (i.e., reduced damping of the microparticles), while low discharge power provides reduced vertical confinement (so that the out-of-plane wave mode can cross with the in-plane mode). Figure 2 shows that the melting of the crystal was triggered in its central region, where the particle density is maximal (i.e., the interparticle distance a is minimal). The melted region then expands outward, eventually encompassing most of the suspended particles.

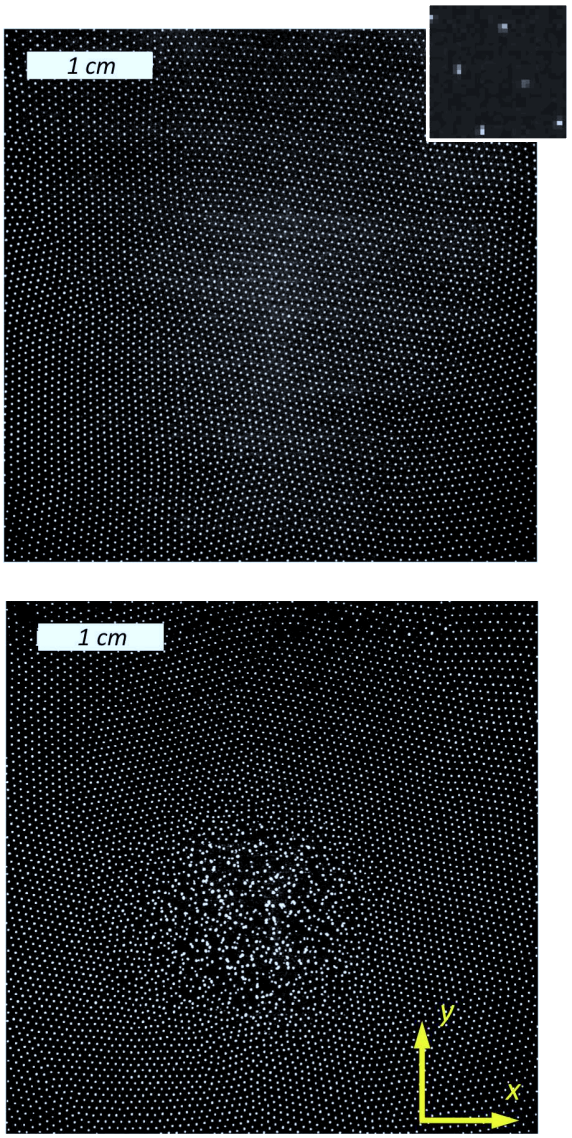

FIG. 2: (color online) Upper panel: Snapshot of the crystal at the beginning of the experiment before the melting starts. Lower panel: Snapshot of a crystal 16.4 s after the beginning of the experiment during the melting phase. The pressure was p =0.4 Pa, the rf power was P=10 W, and the diameter of the dust particle was 9.19 μm. The scale is indicated by the white bar at the top-left corner of each image. The contrast and brightness of the picture were artificially increased and a Gaussian blur was applied to the picture to improve visibility of the dust particles. For reference, a small subregion of the original image is shown in the inset in the upper panel.

B. Particle Image Velocimetry (

For the majority of complex plasma
plasma crystals, particle tracking tech
used very successfully to measure the r
tion of the particles in the crystalline st
the measurements in this experiment, w
sion of previously reported investigatic
al. [15], it is necessary to have simul
ments of particles in both the cryst
regions. To accomplish this, a key fe
periment is the use of Particle Image V
techniques to make measurements of t
ties and to make a clear determinatior
region between the melted and crysta
experiment. PIV is an image analysis t
been used for over a decade in comple
research in a variety of configurations, i
dimensional, [17] stereoscopic, [18] and
configurations. The two-dimensional,
PIV) technique is ideally suited for tl
melting experiments discussed in this
planar PIV analysis techniques applica
ments described in this paper, a pair of
grains that make up the plasma cryst
luminating a single layer of particles v
Each image is then decomposed into
gation cells that are $N \times N$ pixels in
interrogation cell should ideally conta
particles. A cross correlation analysis
ing similar interrogation cells from ea
ing in a two-dimensional cross-correlat
peak in this correlation plane corresp
age displacement of all particles withi
gation cell. If the time interval betwee
is known, then the 2D-PIV technique can be used to construct the average velocity vectors of each group of the particles in the plane of illumination. Figure 3 shows a typical two-dimensional velocity field obtained using the PIV technique. The figure shows that velocity vectors can be obtained over the entire particle cloud.

The goal of this experiment is to identify the characteristic scale length of heat transport across a spatial temperature gradient between crystalline and melted regions in a two-dimensional system. In this analysis, the kinetic energy of the particles - derived from the velocity vectors obtained using the PIV technique - is used as a proxy for the temperature. Measurements of the velocities of the particles are obtained using pairs of images acquired using a Photron FASTCAM. For the measurements recorded at 500 frames/second, every tenth image is used in the PIV analysis (i.e., image 0 and image 10, then image 1 and image 11, etc.). This gives an effective Δt between images of 20 ms. For the measurements recorded at 250 frames/second, every fourth image is used. For this case, the effective Δt between images is 16 ms. In both cases, the interrogation cell used for the velocity reconstruction is a 64×64 pixel region. To improve the spatial resolution of the resulting velocity field, a 75% overlap between interrogation cells is used; that is, a velocity vector is computed at every 16 pixels over the analysis region. First, consider measurements made for the data recorded at 500 frames/second. This experiment was performed with particles having a diameter of 8.77 μm at a neutral gas pressure of $p = 0.9$ Pa. To examine the transition region, velocity vectors are extracted in a horizontal band (i.e. the x-direction in Figure 2) that spans the length of the entire image, from $x = 0$ to $x = 1024$ pixels, located in the band defined by $408 < y < 440$ pixels. This band contains three velocity measurements, at $y = 408$, 424, and 440 pixels, at each horizontal position which are averaged and then used to compute the average kinetic energy of the particles at each horizontal position.

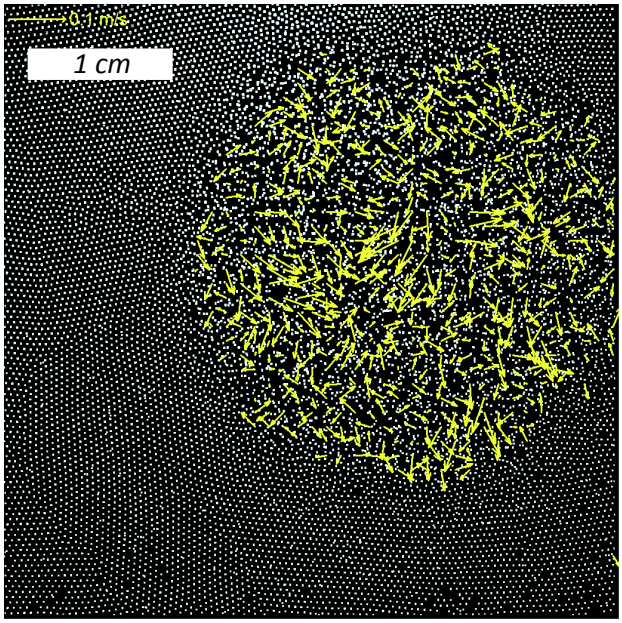

FIG. 3: (color online): Two-dimensional velocity field computed using particle image velocimetry (PIV) technique. The velocity vectors, shown in yellow, are superimposed on an image of the plasma crystal. The larger vectors near the center of the image indicated the higher particle velocities measured in the melted zone.

A time-space plot of the natural logarithm of the kinetic energy (KE) is first computed using the PIV technique, as shown in Fig. 4a, where time advances from $t = 9$ s to $t = 14$ s. The data plotted shows the higher kinetic energy in the melted zone in the center of the image (the lighter or yellow region) and the cooler, crystalline zone at the edges (the darker or red region). As time proceeds, it is shown that the melted region is expanding and eventually encompasses the entire plasma crystal. Furthermore, using the PTV technique (see next section) we were able to calculate the velocity distribution functions inside the melted and crystalline zones, as shown in Figs 4b,c. Finally, the characteristic spatial profile of the kinetic energy is plotted in Fig. 4d.

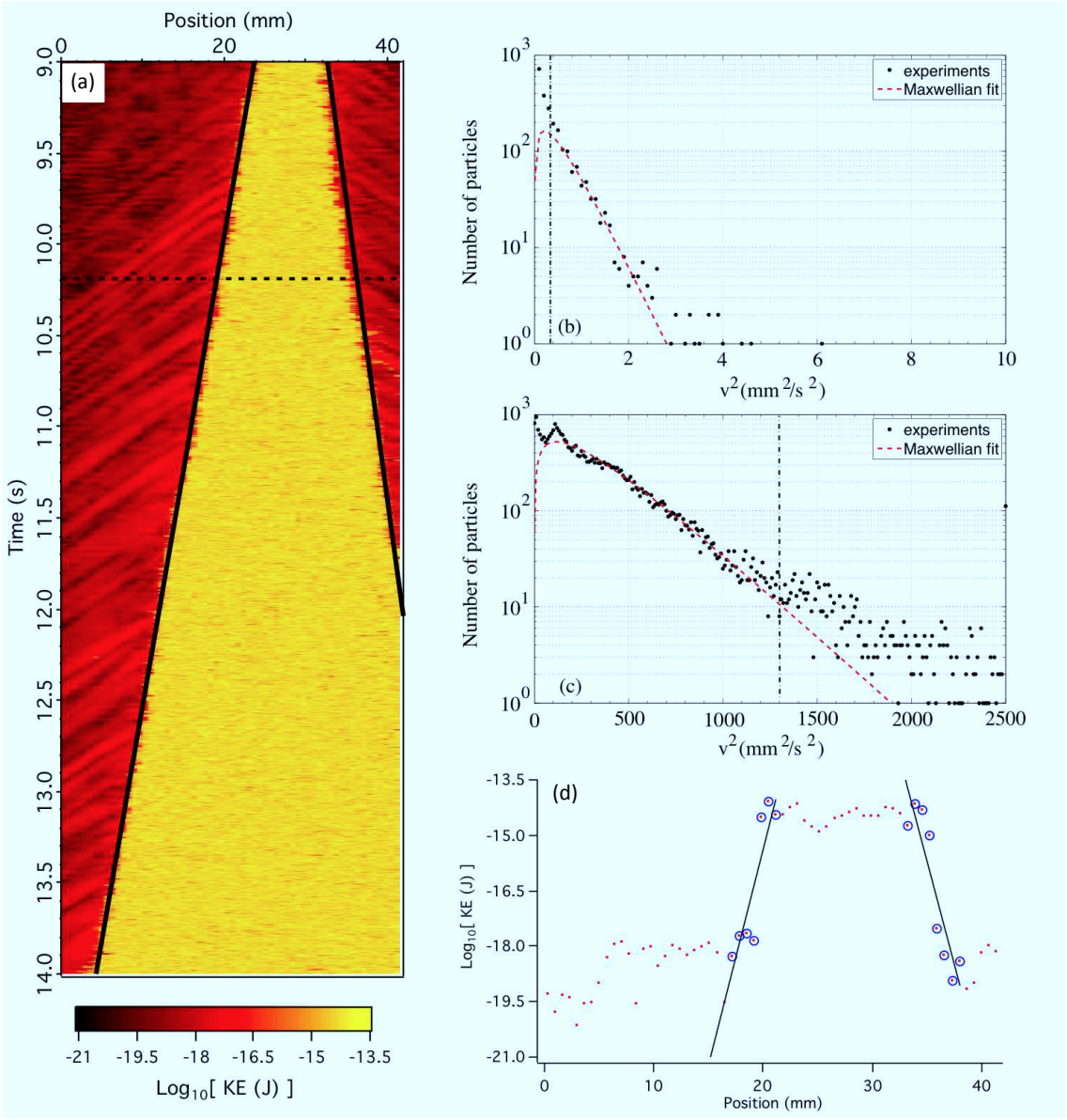

FIG. 4: (color online): (a) A time-space plot of the natural logarithm of the kinetic energy, $\log(KE)$ as a function of time. Time is advancing downward on the left axis from $t = 9$ s to $t = 14$ s. The yellow (lighter) region in the center indicates the higher kinetic energy of the particles in the melted zone. The red (darker) regions at the edges represent the lower kinetic energies of the particles in the crystalline zone. The solid black line indicates the approximate location of the melting front. The velocity distribution functions measured at $t = 10.2$ s [indicated by the horizontal dashed line in (a)] in the crystalline zone (b) and melted zone (c) are also presented. In (b), the frame rate was decreased to 125 fps and the vertical line denotes where the Maxwellian fit was initiated. In (c), the vertical dashed line indicates where the Maxwellian fit is terminated, which corresponds to particles moving more than 1.75 pixel per frame. The spatial profile of the kinetic energy (for the same instant) is plotted in (d).

The spatial gradient of the kinetic energy (temperature) is characterized by the inhomogeneity (gradient) length L_{gr}. An automated process was used to identify the transition from the region of higher to lower kinetic energy (*i.e* the melting front). The identified transition region is denoted by the open circles in Fig. 4d. Once this region was identified, the inhomogeneity (gradient) length L_{gr} is obtained from the general procedure described by Nosenko et al. [24], from the relation given in Eq. 1.

$$\frac{d(KE)}{dx} \propto \exp\left(\frac{x}{L_{gr}}\right). \tag{1}$$

To ensure that the transition region was accurately identified, only transitions that included at least four points (*i.e.*, four measurements of the average velocity)

were required in the transition region were included in the analysis.

The inhomogeneity length, L_{gr}, is computed as a function of time as the plasma crystal melts, for the "left" and "right" fronts shown in Fig. 4d. From the resulting two plots, a distribution of the inhomogeneity lengths is computed for the melting fronts propagating to the left and right. These distributions are fitted to a Gaussian and the peak from the Gaussian fit is used as the transport scale length in the remaining analysis. A summary of these results are presented in Table I.

TABLE I: Summary of experimental measurements to determine the spatial inhomogeneity (gradient) lengths.

Experiment	p Pa	Frame rate fps	L_{gr} (left) mm	L_{gr} (right) mm
1	0.9	500	0.99±0.17	0.95±0.16
2	0.4	250	0.92±0.22	0.88±0.20

C. Particle Tracking Velocimetry (PTV) Analysis: Advantages and Drawbacks

The particle tracking was performed using the PolyParticleTracker software by Rogers *et al.* [21]. The tracking of the dust particles followed these steps: First the image was smoothed in order to reduce the noise, then the particles were identified in order to obtain a first estimate of the particles coordinates followed by a local fit at each feature with a quadratic surface in order to have a sub-pixel refinement of the particle coordinates. Then real particles are dissociated from false track and finally the particle position are linked between frames. A detailed description of the software is given by Rogers *et al.* [21].

The main advantage of PTV is that it gives information about each particle of the studied system. It is nevertheless very expensive in computer time and memory especially for very large system with few thousand particles to track. For that reason the PTV analysis has been limited to small region of the filed of view: a 200×200 pixels zone in both the crystal part and the melted part. These tracking data were used to construct a velocity fluctuation spectrum of the crystal zone (not presented here) in order to extract the longitudinal and transversal acoustic velocities [27] (see Table II) and the kinetic temperature in both regions.

A problem of PTV is pixel locking of particle position. This effect is particularly important when each particle is defined by a very small number of pixels in the original frame (in the presented experiments, the particle area was typically 3-4 pixels). Pixel locking is a very high concern as it can strongly affect the deduced particle velocities. In case of very slow particles, if a particle is moving by less than a pixel and if the sub-pixel refinement of the particle position is not strong enough, it can appear that the particle has not moved at all or moved by one pixel which is wrong in both cases. Camera noise can also artificially move the particles by slightly changing the pixel intensities. For this reason the very slow particles are ignored when fitting the velocity distribution function because their number is overestimated because of the pixel locking. This lower cutoff is denoted by the vertical dashed line in Fig. 4b.

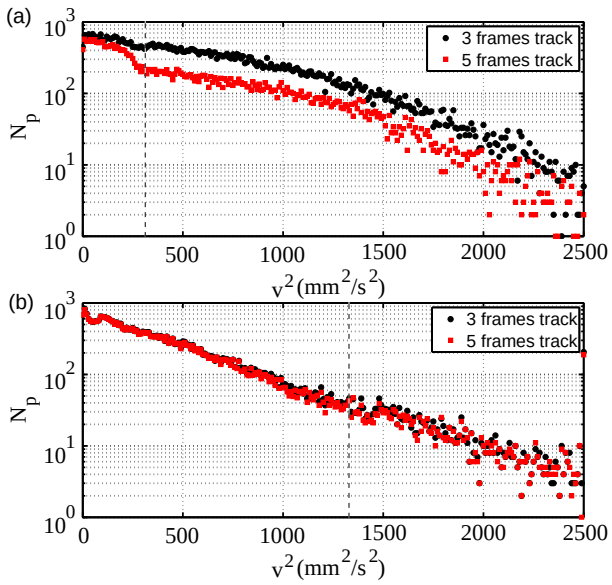

FIG. 5: (color online): PTV velocity distribution of the melted region for two different experimental setups. (a) 250 fps, monolayer is positioned 75 μm below the intensity maximum of the horizontal laser sheet (of Gaussian vertical profile) providing particle illumination. (b) 500 fps, monolayer is positioned at the intensity maximum of the Gaussian profile. In both cases, we applied two filters for the particle tracking. Black circles: a particle must be followed for a minimum of 3 frames. Red squares: a particle must be followed for a minimum of 5 frames.

Moreover, when particles are too fast compared to the chosen frame rate (i.e. the frame rate is too low), the tracking software cannot reconstruct properly the particle track from frame to frame and particles are lost and/or the tracks are mixed giving fake trajectories and thus velocities. This happens typically when the pixel cloud representing a particle in one frame is not partly covered by the pixel cloud of the same particle in the next frame. The software can sometimes guess that the closest found particle is indeed the same but if many particles are in the vicinity the track will be lost. For this reason the part of the velocity distribution function corresponding to a motion of more than 1.5-2 pixel per frame was ignored when fitting the velocity distribution function. This upper cutoff is denoted by the vertical dashed line in Figs. 4c and 5. Furthermore, when particles have be followed for a finite number of consecutive frames they can be lost at this stage. The reason for that is a finite stiffness of the vertical confinement, so that particles can

move vertically and leave the illuminating laser sheet. For example, in Fig. 5, velocity distribution functions are compared for 2 experiments and 2 filters for the particle tracking. As can be seen when the particle is not at the maximum of Gaussian intensity profile (i.e. scattered signal is low and strongly depends on vertical position, Fig. 5a), particles are lost when a minimum of 5 consecutive frames is required to identify a particle track. This does not happen at higher frame rate and for a better scattering signal (Fig. 5b).

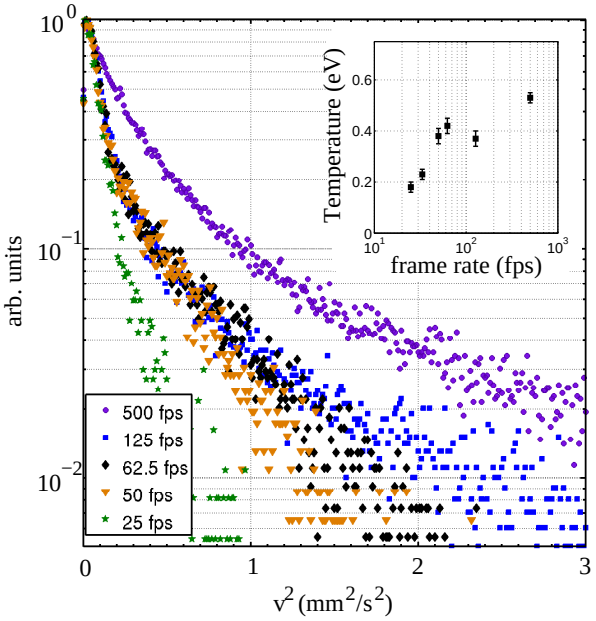

FIG. 6: (color online): PTV velocity distributions for different reduced frame rates in the crystalline zone. The original frame rate was 500 fps. The inset shows the deduced crystal temperature from a fit of the velocity distribution function by a maxwellian distribution function between v^2=0.15 $(\mathrm{mm/s})^2$ and v^2=1.5 $(\mathrm{mm/s})^2$

Finally, when the frame rate is too high compared to the particle mean velocities, the particle velocity distribution function can be hard to recover. Indeed, bad subpixel location of the dust particles and/or camera noise can artificially "move" a particle. On the other hand, when the frame rate is too low, the particle velocities in case of a trapped motion (dust particles in a complex plasma crystal for example) can be artificially lowered: the particle oscillates around its equilibrium position, but the recovered trace does not represent the actual particle trajectory. (If the frame rate is less than twice the highest frequency existing in the wave mode propagating in the crystal, the high frequency component of the particle velocities will be cut out.) It is thus necessary to adapt the frame rate to the studied situation to minimize both effects. This is illustrated in Fig.6. Particles have been tracked in a crystalline monolayer of particles. The original frame rate was 500 fps and we artificiality decreased it by averaging over N consecutive frames before tracking (for example $N = 4$ to decrease the frame rate to 125 fps) As can be seen for the original frame rate the particle velocities are overestimated and the crystal temperature is high ($T \sim 0.5$ eV), for the intermediate frame rate the velocity distribution functions are similar and give a crystal temperature ($T \sim 0.4$ eV). When the frame rate is too low (in our case below 40 fps), the particle velocities are underestimated and the crystal is artificially cold. Consequently the frame rate was decreased to 50 fps to study the crystalline zone and kept at the original one to study the melted zone.

For all these reasons, when one is interested in mean quantities of the particle ensemble, PIV is a better choice as it already gives average values at each grid point without the need of tracking individually each particle (see SectionII B). In general, the PIV technique is a fluid measurement technique and, as such, it is ideally suited to measuring the collective behavior of the microparticles in the plasma. In order to obtain the fluid velocity information, it is necessary to optimize the time between images, Δt, for each interrogation size used in the PIV analysis in order to obtain an accurate measurement of the particle motion of the entire field of view. This process was done prior to applying the PIV technique to the data analyzed in the work presented here. In the analysis of these measurements, the PIV measurement technique readily identifies the wave fronts of the dust lattice waves that are propagating away from the melting zone.

The PIV technique can also be used to measure the fluctuations in the particle velocities, provided the time between the images is sufficiently small, and then the velocity distribution can be reconstructed [19]. Further, a temperature, T, can be also calculated using the second moment of the distribution of velocities in each vector direction using (2) for each PIV measurement.

$$k_B T_{x,y} = m \left\langle \left(v_{x,y} - \langle v_{x,y} \rangle\right)^2 \right\rangle . \qquad (2)$$

where m is the particle mass and k_B is Boltzmann's constant. As can be seen in Fig.4, the kinetic energy of the crystalline zone ($KE \sim 10^{-19.5} - 10^{-19}$ J $\sim 0.2 -$ 0.6 eV) is comparable to the temperature obtained by a Maxwellian fit of the PTV velocity distribution function ($T \simeq$0.4 eV).

III. HEAT TRANSPORT

The mode coupling instability 'tearing' out the structure of the crystalline lattice and melting it, triggers a series of complicated processes of the energy and momentum transport accompanied by the formation of the 'thermal' wave. Even compared to the heat transport in a 2D complex plasma undergoing a phase transition in a mixture of crystalline and liquid phases [24], the heat transport in our conditions is more complicated process. The mean kinetic energy profiles experimentally

measured (see e.g. fig. (4)) demonstrated that the energy transport process undergoes at least three different stages with a principally different transport mechanisms: (i) the 'normal' heat transport at the 'still crystallized' periphery of the lattice layer, (ii) the dominantly radiative transport accompanied by the formation of the intense quasi-regular wave pattern, and (iii) the 'abnormal' heat transport in the central totally melted crystal part showing a 'heat' wave with a sharp front as a fingerprint. To describe this complicated transport pattern in detail from the very beginning is a rather formidable task.

We observed, however, that the melting front quickly became quasi-one-dimensional and quasi-stationary, propagating at an approximately constant speed. It is actually an essential simplification, allowing us to apply as a governing equation of the primitive model proposed and explained in detail by Nosenko et al. in Ref. [24]. Therefore, skipping the details of the routine calculations, we give below the final result only, most interesting for the given study. In the framework of the model of Ref. [24] it is a rather straightforward task to take into account the presence of the stationary heat front. Assuming further that the kinetic energy drops down outside the highly overheated region nearly exponentially, which does not contradict the observations, cf. fig. 4, one can readily derive from the heat transport equation the following relation for the thermal diffusivity χ:

$$\chi = 2\gamma L_{gr}^2 + V_{front} L_{gr}, \tag{3}$$

where γ is the gas friction, L_{gr} is the inhomogeneity (gradient) length [determined by Eq. (1), see also Table I], and V_{front} is the front velocity (determined from Fig. 4). The estimated values of the thermal diffusivity coefficient are collected in Table II. It is remarkable that the major contribution in χ is provided by the second (convective) term in Eq. (3), i.e., the neutral damping plays practically no role in our experiments.

It is worth noting that the thermal diffusivity coefficient obtained here can be considered only as an upper estimate to its real value. This is because the front of the heat wave happened to be anomalously thin, comprising only 1-2 particles on average. The small thickness of the heat front allows one to suggest also another model assuming that the phonons are transported through the thin layer without collisions. An 'effective' thermal diffusivity or the heat transport length L_T in analogy with [28] one can estimate then by using the relationship:

$$\chi \sim V_T L_T, \tag{4}$$

where $V_T = \sqrt{T/m}$ is the thermal velocity of particles and L_T is the heat transport length which is proportional to the gradient length, $L_T \propto L_{gr}$. We note, however, that the mechanism of the heat transport discussed above has to be further developed taking into account more rigorous model for phonon scattering. We save this task for future communications.

IV. CONCLUSIONS

To summarize, we have applied particle image velocimetry and particle tracking techniques to analyze two-dimensional melting in a planar plasma crystal experiment. By combining these techniques, we were able to examine the transport of heat across the temperature gradient layer that exists along a propagating melting front. In particular, we identified the location of the temperature gradient region and found the characteristic scale length for heat transport across this temperature gradient region. It was observed that the melting front quickly became quasi-one-dimensional and quasi-stationary, allowing a simple model for heat transport to be applied. The thermal diffusivity was found to be consistent with previously measured values and determined primarily by the convective term.

Acknowledgments

This work is supported by the U. S. National Science Foundation through grant numbers: PHY-0953595 (J. Williams) and PHY-0810419 (E. Thomas, Jr.). The other authors are supported by: Gefördert von der Raumfahrt-Agentur des Deutschen Zentrums für Luft und Raumfahrt e. V. mit Mitteln des Bundesministeriums für Wirtschaft und Technologie aufgrund eines Beschlusses des Deutschen Bundestages unter dem Förderkennzeichen 50 WP 0203. The research leading to these results has received funding from the European Research Council under the European Union's Seventh Framework Programme (FP7/2007-2013) / ERC Grant agreement 267499.

TABLE II: The Epstein damping rate γ, the number of particles in the field of view of the camera N_p, the particle charge number Z, the lattice constant a, the screening parameter κ, the front characteristics V_{front} and L_{gr}, thermal diffusivity χ, and the heat transport length L_T.

Experiment	γ s^{-1}	N_p	Z	κ mm	a mm/s	V_{front} mm	L_{gr} mm^2/s	χ eV	T mm/s	V_T	V_{front}/V_T
1	1.13	$\simeq$11000	12300	1.3	0.43	4.0	1.0 [a]	6.1 [a]	460	11.8	0.3
2	0.48	$\simeq$6000	16200	1.0	0.57	6.6	0.9 [a]	6.7 [a]	170-800 [b]	6.7-14.5	0.4-1

[a] upper estimate; the measurement uncertainty stems from the finite bin size/interparticle distance;
[b] obtained by PTV. The first and the second datasets are not identical in the particle registration method. The "shifted" illumination at 250 fps (Exp. 2) gives a very noisy data that makes the particle velocity distribution measurements highly uncertain.

[1] C. Goertz, Rev. Geophys, **27**, 271 (1989).
[2] D. A. Mendis and M. Rosenberg, Ann. Rev. Astron. Astrophys., **32**, 419 (1994).
[3] A. L. Graps, E. Grün, H. Svedhem, H. Krüger, M. Horányi, A. Heck, and S. Lammers, Nature, **405**, 48 (2000).
[4] D. A. Gurnett, E. Grn, D. Gallagher, W. S. Kurth, and F. L. Scarf, Icarus, **53**, 236 (1983).
[5] A. Barkan, N. D'Angelo, and R. L. Merlino, Phys. Rev. Lett., **73**, 3093 (1994).
[6] B. Walch, M. Horanyi, and S. Robertson, Phys. Rev. Lett., **75**, 838 (1995).
[7] M. S. Barnes, J. H. Keller, J. C. Forster, J. A. O'Neill, and D. K. Coultas, Phys. Rev. Letters, **68**, 313 (1992).
[8] A. Barkan and R. L. Merlino, Phys. Plasmas, **2**, 3261 (1995).
[9] T. Nitter, Plasma Sources Sci. Technol., **5**, 93 (1996).
[10] J. H. Chu and Lin I, Phys. Rev. Lett., **72**, 4009 (1994).
[11] H. Thomas, G. E. Morfill, V. Demmel, J. Goree, B. Feuerbacker, and D. Mölmann, **73**, 652 (1994).
[12] O. Arp, D. Block, A. Piel, and A. Melzer, Phys. Rev. Lett., **93**, 165004 (2004).
[13] A. V. Ivlev and G. Morfill, Phys. Rev. E **63**, 016409 (2000).
[14] A. V. Ivlev, U. Konopka, G. Morfill, G. Joyce, Phys. Rev. E **68**, 026405 (2003).
[15] L. Couëdel, V. Nosenko, A. V. Ivlev, S. K. Zhdanov, H. M. Thomas, and G. E. Morfill, Phys. Rev.Lett., **104**, 195001 (2010).
[16] L. Couëdel *et al.*, Phys. Plasmas **18**, 083707 (2011).
[17] E. Thomas, Jr., Phys. Plasmas, **6**, 2672 (1999).
[18] E. Thomas, Jr., J. Williams, and J. Silver, Phys. Plasmas, **11**, L37 (2004).
[19] J. Williams and E. Thomas Jr, Phys. Plasmas **14**, 063702 (2007).
[20] J. Williams, Phys. Plasmas, **18**, 050702 (2011).
[21] S. S. Rogers, T. A. Waigh, X. Zhao, J. R. Lu, Phys. Biol. **4**, 220-227 (2007)
[22] S. K. Zhdanov et. al., Phys. Plasmas, **16**, 083706 (2009).
[23] B. Liu, J. Goree, Y. Feng, Phys. Rev. Lett. **105**, 085004 (2010).
[24] V. Nosenko et al., Phys. Rev. Lett. **100**, 025003 (2008)
[25] V. Nosenko et al., Phys. Plasmas **13**, 032106 (2006)
[26] S. Nunomura, D. Samsonov, S. Zhdanov, and G. Morfill, Phys. Rev. Lett. **95**, 025003 (2005).
[27] S. Nunomura, J. Goree, S. Hu, X. Wang, A. Bhattacharjee, and K. Avinash, Phys. Rev. Lett. 89, 035001 (2002).
[28] L. D. Landau and E. M. Lifshitz *Fluid Mechanics* (Pergamon, 1963).